Study on dynamic performance of SOFC

Haiyang Zhan*, Qianchao Liang, Qiang Wen and Runkai Zhu

Naval University of Engineering, Wuhan 430033, China

*Corresponding author e-mail:13349923382@163.com

Abstract. In order to solve the problem of real-time matching of load and fuel cell power, it is urgent to study the dynamic response process of SOFC in the case of load mutation. The mathematical model of SOFC is constructed, and its performance is simulated. The model consider the influence factors such as polarization effect, ohmic loss. It also takes the diffusion effect, thermal effect, energy exchange, mass conservation, momentum conservation. One dimensional dynamic mathematical model of SOFC is constructed by using distributed lumped parameter method. The simulation results show that the I-V characteristic curves are in good agreement with the experimental data, and the accuracy of the model is verified. The voltage response curve, power response curve and the efficiency curve are obtained by this way. It lays a solid foundation for the research of dynamic performance and optimal control in power generation system of high power fuel cell stack.

1. Introduction

Solid oxide fuel cells can convert chemical energy directly into electrical energy, which breaks the limitation of the cycle thermal efficiency of Kano. It has the incomparable efficiency of traditional heat engine, and the combined cycle efficiency of thermal power is as high as 50% [1]. The application of fuel cell in the next generation distributed generation device and portable mobile power supply has the advantages of high efficiency, environmental protection, safety and so on. SIEMENS in 2000 to achieve the 100kW level of the fuel cell stack power generation system running [2], but the majority of domestic fuel cell stack is still in the theoretical stage.

At present, the technology of SOFC is not mature, and the price is very high. When the load changes, it will cause the irreversible loss of the fuel cell plate. In order to solve the load and fuel cell power real-time matching problem, the urgent need to explore the high temperature solid oxide fuel cell dynamic response process of mutation in the load; urgent need construct a simple, accurate and reliable mathematical model, saving the cost, shorting the test cycle. In this paper, a one-dimensional mathematical model is established, which lays a solid foundation for the design of the stack structure and the construction of the combined power generation system [3].

2. Constructing mathematical model

The fuel cell plate is divided into three layers: anode, electrolyte and cathode. The energy of any node in the stack is:

$$E_{\text{total}} = \Delta H \cdot I / nF \tag{1}$$

The output power in the form of electricity, can be expressed as:

$$W = -IV \tag{2}$$

The heat loss of the node is:

$$Q = \Delta H \cdot I / nF - W \tag{3}$$

It is concluded that the loss of the heat dissipation is the formation of polarization heat generation and entropy production. Using the polarization, diffusion, forced convection heat transfer, mass conservation and other factors as the constraint conditions, the iterative algorithm is used to reduce the error [4]. The logical structure of the mathematical model is shown in Figure 1:

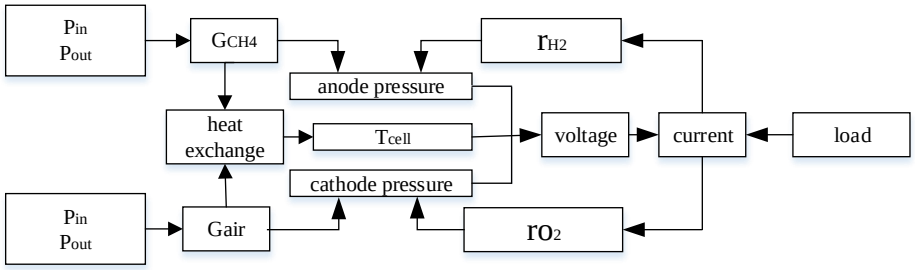

Figure 1. Schematic diagram of fuel cell mathematical model

2.1. Reformer model

The fuel gas of the fuel cell stack is methane and steam reforming reaction mixture, and the steam -to-carbon ratio should be greater than 3 in order to ensure that no carbon deposition phenomenon, There are two reversible reactions in the reformer under the action of catalyst [5]:

$$CH_4 + H_2O \leftrightarrow CO + 3H_2,\ \Delta H = 206.2\ \text{KJ/mol} \tag{4}$$

$$CO + H_2O \leftrightarrow CO_2 + H_2,\ \Delta H = -41.2\ \text{KJ/mol} \tag{5}$$

The rate of methane consumption was determined by reforming reaction rate:

$$r_r = K_r P^{\alpha}_{CH_{4,tpb}} P^{\beta}_{H_2O,tpb} \exp\left(-\frac{E_r}{RT_{fuel}}\right) \tag{6}$$

Reforming coefficient α=0.85, β= -0.35, activation energy of reforming reaction Er=95 kJ/mol, Reforming reaction rate coefficient Kr=8542. The residual amount of methane in the exhaust gas can be neglected, and the reforming reaction of methane reaches equilibrium state [6]:

$$K_r = \exp\left(A_r T^4_{fuel} + B_r T^3_{fuel} + C_r T^2_{fuel} + D_r T_{fuel} + E_r\right) \tag{7}$$

The reaction speed is faster and the equilibrium state is more rapid than reforming reaction [7]:

$$K_s = \exp\left(A_s T^4_{fuel} + B_s T^3_{fuel} + C_s T^2_{fuel} + D_s T_{fuel} + E_s\right) \tag{8}$$

2.2. Electrochemical model

Electrochemical reactions are as follows in the anode and cathode [8]:

$$H_2 + O^{2-} \rightarrow H_2O + 2e^- \tag{9}$$

$$\frac{1}{2}O_2 + 2e^- \rightarrow O^{2-} \tag{10}$$

The experimental results show that the electrochemical reaction is extremely fast enough to consume all reactants reaching the reaction interface [9]. The voltage of SOFC can be expressed by the Nernst equation:

$$E^0 = 1.2723 - 2.7645 \times 10^{-4} T_{\text{cell}} \tag{11}$$

Actual stack voltage:

$$v_{\text{fc}} = E - \eta_{\text{ohmic}} - \eta_{\text{conc}} - \eta_{\text{act,a}} - \eta_{\text{act,c}} \tag{12}$$

Ohmic polarization indicates the resistance of electrons to the electrolyte; Concentration difference polarization indicates that the polarization resistance formed by the transfer process of the gas phase material through the electrode can be observed only under the high current density or the low concentration of the segregation; Anode activation polarization and cathode activation polarization indicate that the electrochemical reaction must overcome an energy barrier for the activation energy of the reaction[10].

2.3. Diffusion Model

The diffusion process plays an important role in the process of dynamic response. This is because the actual reaction takes place in the three-phase interface layer, and the reactants must diffuse through the porous electrode to the three-phase interface layer. In the first phase the material flow must pass through the interface layer to the surface of the electrode; in the second stage, the material flows through the porous electrode to the reaction interface [11]. Diffusion are major means of transmission, and the driving force of diffusion is a concentration gradient, Fick's law shows that [12]:

$$\frac{\partial C}{\partial t} = -D\frac{\partial^2 C}{\partial x^2} \tag{13}$$

The diffusion coefficient can be used to express the diffusion velocity, and the pressure of the gas components in the three-phase interface can be obtained:

$$P_{\text{H}_2,\text{tpb}} = P_{\text{H}_2} - \frac{RTl_{\text{a}}I}{2FD_{\text{eff(a)}}} \tag{14}$$

$$P_{\text{O}_2,\text{tpb}} = P_{\text{air,in}} - (P_{\text{air,in}} - P_{\text{O}_2}) \times \exp\frac{RTl_{\text{c}}I}{4FD_{\text{eff(c)}}P_{\text{air,in}}} \tag{15}$$

Anode plate channel gas contains CH_4, CO, CO_2, H_2, and H_2O. The material flow constraints are obtained by mass conservation:

$$\frac{\mathrm{d}G_i}{\mathrm{d}t} = A_{\mathrm{a}} \frac{P_{\mathrm{fuel,in}}}{RT_{\mathrm{fuel,in}}} u_{\mathrm{fuel,in}} x_{i,\mathrm{in}} - A_{\mathrm{a}} \frac{G_i}{dV_{\mathrm{a}}} u_{\mathrm{fuel}} + R_i \tag{16}$$

$$R_i = [-r_{\mathrm{r}}; r_{\mathrm{r}} - r_{\mathrm{s}}; r_{\mathrm{s}}; 3r_{\mathrm{r}} + r_{\mathrm{s}} - r_3; -r_{\mathrm{r}} - r_{\mathrm{s}} + r_3] \tag{17}$$

$$\frac{\mathrm{d}G_{\mathrm{O_2}}}{dt} = A_{\mathrm{c}} \frac{P_{\mathrm{air,in}}}{RT_{\mathrm{air,in}}} u_{\mathrm{air,in}} x_{\mathrm{O_2,in}} - A_{\mathrm{c}} \frac{G_{\mathrm{O_2}}}{dV_{\mathrm{c}}} u_{\mathrm{air}} - r_3 \tag{18}$$

Here r is electrochemical reaction rate.

2.4. Temperature Model

The fuel cell plate is very thin along the radial direction, and the temperature difference is very small. There is a temperature gradient along the direction of the flow, but the temperature of the reactor cannot be measured directly. The average temperature of the outlet is used as the temperature of the cell [13]. The main heat transfer in the fuel cell is the forced convection in the gas flowing through the channel:

$$q_{\mathrm{conv}} = hA\left(T_{\mathrm{cell}} - T_{\mathrm{fuel}}\right) \tag{19}$$

Here h is convective heat transfer coefficient; A is heat exchange area; Tcell is plate temperature; Tfuel is gas temperature. The experimental results show that the gas flow in the channel is laminar, and the Reynolds number of the anode and cathode channel is 66 and 287. The relationship between Reynolds and Planck is used to determine the heat transfer coefficient:

$$m_{\mathrm{cell}} C_{\mathrm{cell}}\left(T\right) \cdot \frac{\mathrm{d}T_{\mathrm{cell}}}{\mathrm{d}t} = -P_{\mathrm{fc}} - r_3 \Delta H_3\left(T\right) - q_{\mathrm{conv}} \tag{20}$$

$$\begin{aligned} C_{\mathrm{re}}\left(T\right) \cdot \frac{\mathrm{d}T_{\mathrm{out}}}{\mathrm{d}t} = {} & \sum\left(G_{\mathrm{in},i}^{\mathrm{air}} \cdot h_{\mathrm{in},i}^{\mathrm{air}}\right) + \sum\left(G_{\mathrm{in},i}^{\mathrm{fuel}} \cdot h_{\mathrm{in},i}^{\mathrm{air}}\right) - \sum\left(G_{\mathrm{out},i}^{\mathrm{air}} \cdot h_{\mathrm{out},i}^{\mathrm{air}}\right) - \\ & \sum\left(G_{\mathrm{out},i}^{\mathrm{fuel}} \cdot h_{\mathrm{out},i}^{\mathrm{fuel}}\right) - r_{\mathrm{r}} \Delta H_{\mathrm{r}}\left(T\right) - r_{\mathrm{s}} \Delta H_{\mathrm{s}}\left(T\right) + q_{\mathrm{conv}} \end{aligned} \tag{21}$$

Here P_{fc} Output power.

Based on the above analysis, the dynamic simulation model of fuel cell is shown in Figure 2:

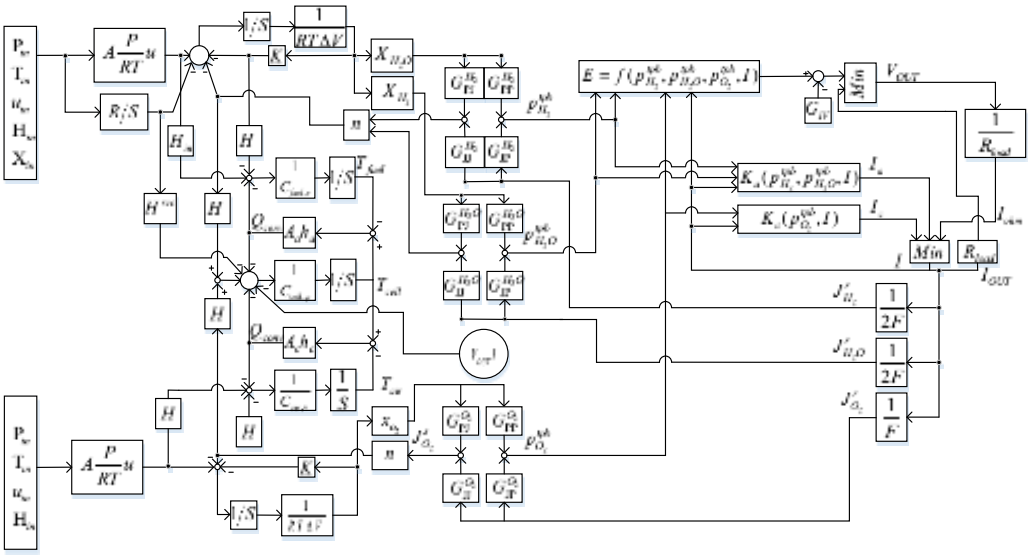

Figure 2. Schematic diagram of dynamic model

3. Dynamic performance analysis

3.1. Test data

In this paper, 30 identical fuel cell plates are used to form a stack. The anode of cell is negative electrode, and the cathode is positive electrode. The collector is a double-layer silver mesh to increase the electrical conductivity between the junction and the stack electrode. Sealing ring is used for sealing anode and bottom connection, same as cathode and top connector. Specific structure is shown in Figure 3, 4:

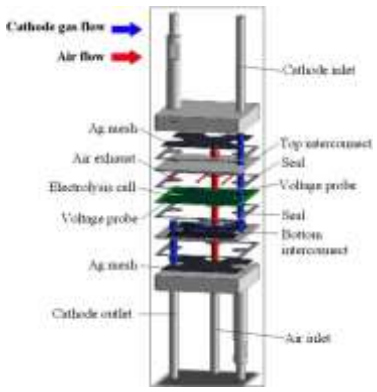

Figure 3. The structure of reactor connection

Figure 4. Fuel cell structure

The test system is composed of three modules: monitoring system, reforming control system and stack system:

Figure 5. Experimental test system

The experiment was carried out by using the methane flow rate 3.5SLM, the excess air 58SLM, the steam-to-carbon 3, and the constant current discharge mode of electronic load. Specific experimental parameters are shown in Table 1:

Table 1. Experimental parameters

Parameter	Numerical value	Note
$P_{air,in}$	11.7 kPa	Cathode side air inlet gauge pressure
$P_{fuel,in}$	6 kPa	Anode side CH_4 inlet gauge pressure
G_{CH4}	3.5 SLM	Reformer inlet CH_4 flow rate
G_{air}	58 SLM	Cathode side inlet air flow
G_{H2O}	8.435 ml/min	Reformer inlet water flow
T_{cell}	732.2℃	Stack mean temperature
P_{sofc}	388kg/cm^2	Sealed fuel cell stack pressure
N	30	The stack consists of 30 identical plates

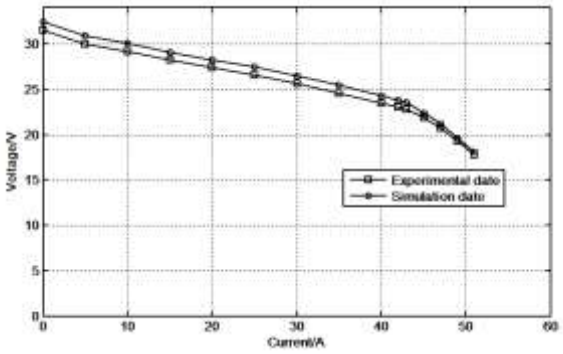

Figure 6. V-A characteristics

It is concluded from Fig. 6 that the polarization loss leads to the nonlinearity of the volt ampere characteristic in the initial stage, and then the ohmic loss is dominant. When the discharge current is large, the reactant is too late to diffuse into the three-phase interface layer, which makes the polarization of the concentration difference cause great loss to the voltage. In the process of increasing current, the simulation results are basically consistent with the experimental data. It is good to reflect the change law, and the maximum error is only 2.3%.

The experimental test was carried out on 30 pieces of plate type fuel cells produced by the SOFC company. The experimental results show that the characteristic curves of cell are obtained under different CH_4 flow rate, as shown in figure 7-9:

Table 2. Experimental parameters

Number	1	2	3	4
G_{CH4}	3 SLM	3.5 SLM	3.9 SLM	4.4 SLM
G_{air}	40 SLM	46.6 SLM	52 SLM	58.6 SLM
G_{H2O}	7.23ml/min	8.4 ml/min	9.4 ml/min	10.6 ml/min
T_{cell}	748℃	748℃	748℃	748℃

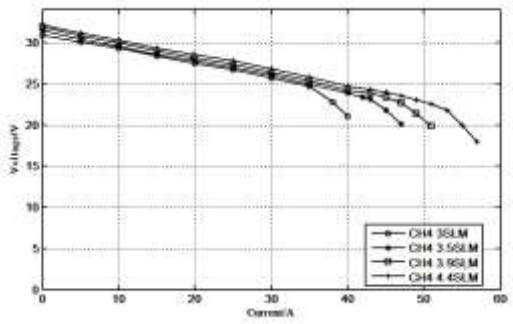

Figure 7. V-A characteristics curve

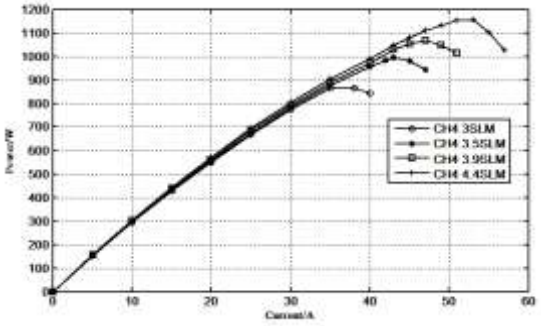

Figure 8. Power characteristic curve

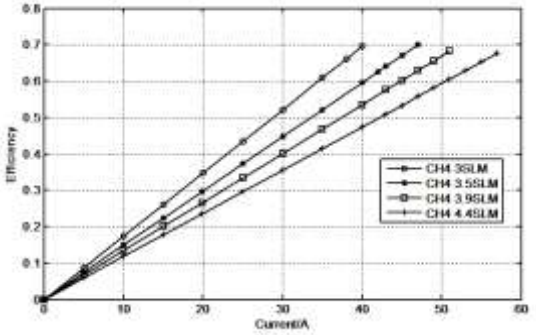

Figure 9. Characteristic curve of fuel utilization

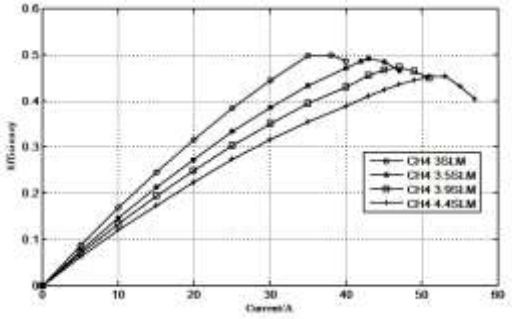

Figure 10. Efficiency characteristic curve

Figure 7-9 shows that the voltage attenuation is alleviated with the increase of methane flow rate. The power increases first and then decreases with the increase of current. The fuel utilization rate increases with the increase of the discharge current, but the excessive fuel utilization will lead to the irreversible decay of the cell. The experimental fuel utilization rate is controlled within 65%. When the power reaches the maximum, the electrical efficiency reaches the maximum value. When the fuel utilization ratio is 60%~65%, the power reaches the maximum, and the electrical efficiency reaches 48%~50%.

3.2. Dynamic performance simulation

In the simulation of dynamic performance, the discharge current is simulated by 5A, 10A, 15A, 20A, 25A, 30A, 35A, 40A, 43A for 60 seconds. Simulation of dynamic response process as shown in figure 11-13:

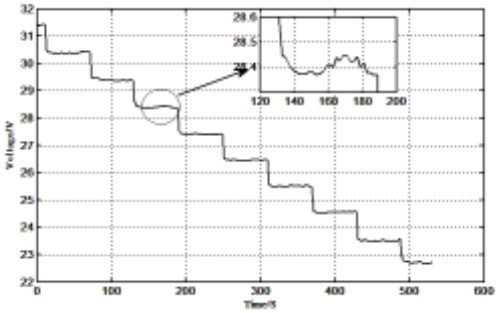

Figure 11. Voltage dynamic response process

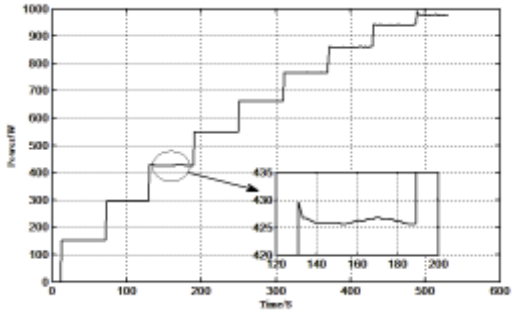

Figure 12. Power response process

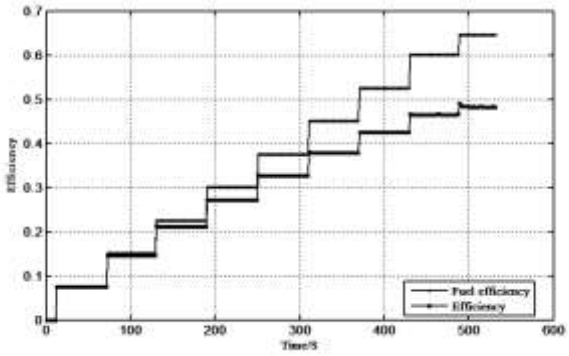

Figure13. Efficiency response process

Figure 11-13 shows that the existence of hysteresis in the voltage response. Because the electric double layer capacitance on the interface between the ion conductor and the electron conductor leads to the voltage cannot change suddenly. With the increase of the discharge current, the loss of cell increases and the voltage decreases. Due to the decrease of the fuel concentration in the three-phase interface layer, the diffusion effect is enhanced. At the same time, increasing the discharge current will cause the cell temperature to rise, and the voltage will increase slightly. With the increase of the discharge current, the power increases at the same time, but the power will have a certain amount of overshoot. The fuel utilization efficiency and the electric efficiency increase with the increase of the discharge current.

In the simulation of dynamic performance, the discharge current is simulated by 43A, 40A, 35A, 30A, 25A, 20A, 15A, 10A, 5A for 60 seconds. Simulation of dynamic response process as shown in figure 14-15:

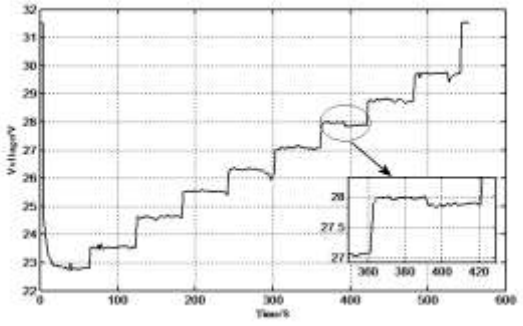

Figure 14. Voltage dynamic response process

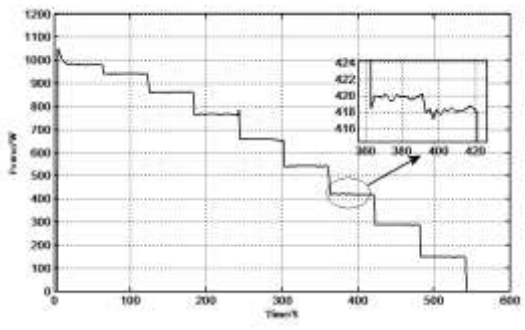

Figure 15. Power response process

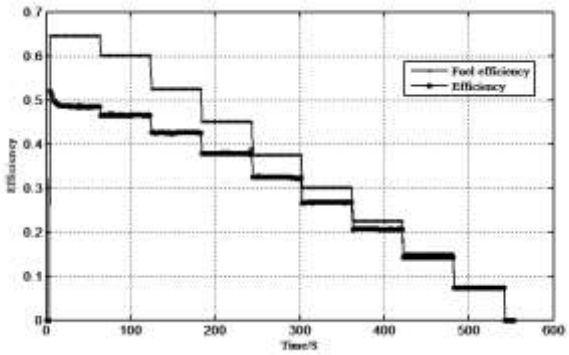

Figure 16. Efficiency response process

Figure 14-16 shows that the voltage response also has hysteresis, when the discharge current is reduced. The reduction of the discharge current will reduce the cell loss, so that the voltage can be improved. At the same time, the small current discharge will cause the decrease of the cell temperature, which makes the voltage drop slightly. Power, fuel utilization and electrical efficiency decrease with the decrease of discharge current.

4. Conclusion

Based on the mathematical model of fuel cell established in this paper, the simulation results are in good agreement with the experimental data, and the reliability of the model is verified. In this paper, when the fuel utilization ratio is 60%~65%, the power and the efficiency reach the maximum; When the discharge current increases, the voltage response has hysteresis, which will cause the transient overshoot of power; When the discharge current is reduced, the voltage response is delayed, which results in the decrease of temperature. In order to realize the real-time matching of power and load, it is the most feasible way to adjust the methane flow rate. By studying the dynamic response process of the cell, it provides a way to solve the problem of load and power real-time matching. At the same time, it can lay a good foundation for the popularization and application of fuel cell distributed generation equipment.

Acknowledgments

Thanks to the support of the Hubei Innovation Fund Project (HX2015B1003) and the 12th Five-Year Defense Advanced Research Foundation (No.40103030403).

References

[1] Bove R, Lunghi P, Sammes NM. SOFC mathematic model for systems simulation –Part2: Definition of an analytical model [J]. International Journal of Hydrogen Energy, 2005, (30): 189-200.
[2] Wu XJ, Zhu XJ, Cao GY, Tu HY. Predictive control of SOFC based on a ga-rbf neural network model [J]. Journal of power Energy, 2008, 179(1): 232-239.
[3] Yang J, Li X, Mou HG, Jian L. Predictive control of solid oxide fuel cell based on an improved takegi-sugeno fuzzy model [J]. Journal of power Energy, 2009, 193(2): 699-705.
[4] L Jin, WB Guan, X Ma, C Xu, WG Wang, A chieving hydrogen production through solid oxide electrolyzer sack by high temperature electrolysis [J]. ECS, 2012(41): 103-111.
[5] Florian Leucht, Wolfgang G. Bessler. Fuel cell system modeling for solid oxide fuel cell/gas turbine hybrid power plants, Part I: Modeling and simulation framework [J]. Journal of Power Sources, 2011 (196): 1205–1215.
[6] Yifeng Zheng, Qingshan Li, Wanbin Guan, Cheng Xun, WeiWu, WeiGuo Wang. Investigation of 30-cell solid oxide electrolyzer stack modules for hydrogen production [J]. Journal of

Power Energy, 2014(40): 5801-5809.
[7] Qingshan Li, Yifeng Zheng, Wanbing Guan, Le Jin, Cheng Xu, Wei Guo Wang. Achieving high-efficiency hydrogen production using planar solid-oxide electrolysis stacks [J]. Journal of Power Energy, 2014(39): 10833-10842.
[8] Le Jin, Wanbing Guan, Xiao Ma, Huijuan Zhai, Wei Guo Wang. Quantitative contribution of resistance sources of components to stack performance for planar solid oxide fuel cells [J]. Journal of Power Energy, 2014(253): 305-314.
[9] Guan WB, Zhai HJ, Jin L, Xu C, Wang WG. Temperature measurement and distribution inside planar SOFC stacks [J]. Fuel cells, 2012, 12(1): 24-31.
[10] Tan Xun-qiong, Wu Zheng-qiu, Zhou Ye, Zhong Hao, Li Jun-jun. Solid Oxide Fuel Cell Lumped Modeling and Simulation [J]. Proceedings of the CSEE, 2010, 6(17): 104-110(in Chinese).
[11] Tang Gen-tu, Luo Zhong-yang, Ni Ming-jiang, Yu Chun-jiang, Cen Ke-fa. Numerical simulation and performance analysis of planar anode-supported solid oxide fuel cell [J]. Proceedings of the CSEE, 2005, 5(10): 116-121 (in Chinese).
[12] Sun Xiu-yu, Wang Hao. Dynamic modeling and predictive control of solid oxide fuel cell [M]. Beijing: China Machine Press, 2015:153-173 (in Chinese).
[13] Lu Xiao-Jing, Lu Chao-Hao, Geng Xiao-Ru, Zhu Xin-Jian, Weng Yi-Wu. Effect of Steam on the Performance of an IT-SOFC/GT Hybrid System [J]. Journal of engineering thermal physics, 2016, 4(4): 705-710 (in Chinese